AC Performance of Flexible Transparent InGaZnO Thin-Film Transistors and Circuits

Federica Catania, Mukhtar Ahmad, Dianne Corsino, Niloofar Saeedzadeh Khaanghah, Luisa Petti, *Senior Member, IEEE*, Niko Münzenrieder, *Senior Member, IEEE*, and Giuseppe Cantarella, *Member, IEEE*

***Abstract*— Transparent transistors are mainly investigated in view of their integration in displays and their employment in wearable electronics where the integration of flexible and imperceptible systems is an important requirement. Here, the fabrication and ac performance of flexible InGaZnO thin-film transistors (TFTs) and circuits are presented to evaluate their suitability for analog sensor conditioning applications. Functional oxides are employed to guarantee the transparency of the device, while their fabrication processes are suitable to directly realize electronics on a flexible polyimide substrate. The TFTs show state-of-the-art performance with a field-effect mobility $\mu_{eff} = 19.39\ cm^2V^{-1}s^{-1}$ and functionality while bent to radii as low as 5 mm. Reliable scattering parameters measurements confirm transit frequencies as high as $f_t \approx 7.84$ MHz. Simultaneously, nMOS ring oscillators (ROs) show functionality at supply voltage V_{DD} ranging from 1.75 to 12.25 V with a maximum oscillation frequency $f_{osc} = 132.9$ kHz. Finally, common-source amplifiers (CSAs) exhibit the voltage gains up to 10.7 dB, the cutoff frequencies up to 10.8 kHz, and a power consumption down to 4.4 μW.**

***Index Terms*— AC performance, flexible electronics, InGaZnO, thin-film transistors (TFTs), transparent electronics.**

I. Introduction

THIN-FILM electronics on flexible substrates have recently attracted increasing interest because of the special characteristics of lightweight, large-area compatibility, scalability, low-cost production, and mechanical bendability [1]. This combination of properties, enabled by the use of advanced materials and processes [2], has paved the way for new applications in different fields, such as sensing technologies [3], smart textiles [4], and healthcare systems [5]. In addition to the mechanical properties of thin-film electronics, transparency has been gaining relevance for the development of unobtrusive skin patches [6], displays [7], and electrodes for solar cells [8]. For the realization of thin-film electronics, metal oxide semiconductors, such as amorphous indium–gallium–zinc–oxide (a-IGZO) [9], provide high electron mobility [10], large processability, optical transparency, and low-temperature deposition techniques compatible with flexible polymeric substrates [11]. To achieve high transmittance in the whole device stack, IGZO is combined with transparent oxide conductors, such as indium–tin–oxide (ITO) [12]–[17], aluminum–zinc–oxide (AZO) [18], indium–zinc–oxide (IZO) [19], or metals, such as molybdenum (Mo) [20], [21]. Their dc performance is reported, whereas information on their ac performance is only presented for transparent thin-film transistors (TFTs) fabricated on rigid glass substrate [21] or acquired from only partially transparent flexible devices [22]. The frequency performance of transparent IGZO TFTs has mainly been investigated utilizing ring oscillators (ROs) [13], [20], [23]. These circuits showed operating frequencies up to 2.1 MHz when fabricated on a glass substrate [13], whereas flexible circuits, released from a rigid carrier after the device fabrication, exhibited lower operating frequencies (94.8 kHz [20] and 182 kHz [23]). Similarly, other transparent IGZO logic circuits directly fabricated on either rigid glass [13], [16] or flexible substrates [19], [23] have been presented. However, flexible and transparent analog circuits have never been reported. In this study, the performance of transparent oxide thin-film electronics, consisting of TFTs and analog circuits fabricated on a flexible polyimide substrate, is investigated. The devices are fabricated exclusively employing transparent materials: IGZO semiconducting layer, aluminum oxide (Al_2O_3) insulating layer, and ITO contacts. The dc performance of single flat and bent TFTs is evaluated, whereas the TFT ac performance is obtained from scattering parameters measurements. In addition, fully integrated-based five-stage ROs and, for the first time to the best of our knowledge, transparent common-source amplifiers (CSAs) are demonstrated and characterized, to evaluate their suitability as front-end sensor conditioning circuits for wearable and health devices.

Manuscript received 20 May 2022; revised 18 July 2022; accepted 18 July 2022. Date of publication 27 July 2022; date of current version 23 August 2022. This work was supported in part by the European Regional Development Fund (ERDF) Program, Autonomous Province of Bozen-Bolzano-South Tyrol, under Project the Europäischer Fond für regionale Entwicklung/Fondo europeo di sviluppo regionale (EFRE/FESR) 1140-PhyLab and Project EFRE/FESR 1068-Senslab; in part by the International Joint Cooperation South Tyrol-Switzerland Swiss National Foundation (SNF) [Flexible Electronics meets μ-Robotics (FLEXIBOTS)], Autonomous Province of Bozen-Bolzano/South Tyrol, under Grant 2/34; in part by the Free University of Bozen [(ricercatore/ricercatrice a tempo determinato (RTD) Call Faculty of Science and Technology (FAST) 2020, Flexible Electronics-integRated Micromachines (FERMI)]; and in part by the Deutsche Forschungsgemeinschaft (DFG) FFlexCom Initiative, Germany, through the Project Wireless Indium-Gallium-Zinc-Oxide Transmitters and Devices on Mechanically Flexible Thin-Film Substrates II (WISDOM II), under Grant 271795180. The review of this article was arranged by Editor J. F. Conley. *(Corresponding author: Federica Catania.)*

The authors are with the Faculty of Science and Technology, Free University of Bozen-Bolzano, 39100 Bolzano, Italy (e-mail: fecatania@unibz.it).

Color versions of one or more figures in this article are available at https://doi.org/10.1109/TED.2022.3193012.

Digital Object Identifier 10.1109/TED.2022.3193012

II. Materials and Device Fabrication

Bottom-gate inverted staggered IGZO TFTs and circuits were directly fabricated on free-standing 7-cm × 7-cm large polyimide foil using vacuum deposition processes and standard UV lithography.

A. Fabrication

All devices and circuits were fabricated on free-standing 50-μm-thick polyimide substrate, as shown in Fig. 1(a). The plastic foil was cleaned with acetone and isopropanol in an ultrasonic bath for 5 min, respectively, and dried at 200 °C for 24 h. Then, the front and back of the polymeric substrate were encapsulated with 50-nm-thick SiN_x using a plasma-enhanced chemical vapor deposition (PECVD) process. The resulting buffer layer improves the adhesion of the device stack, minimizing the absorption of liquids and, hence, swelling of the substrate during the fabrication process, and reduces outgassing speeding up pumping times in vacuum chambers. The first step of TFTs and circuits fabrication process itself was the deposition of a 55-nm-thick bottom gate ITO layer using RF sputtering and liftoff structuring. Then, 25-nm-thick Al_2O_3 was grown by atomic layer deposition (ALD) at 150 °C with no other postdeposition treatments. This was the maximum temperature reached during the fabrication process. The semiconducting active layer consisted of 15-nm-thick a-IGZO deposited at room temperature by RF sputtering. Both the IGZO layer and the Al_2O_3 layer were structured by the UV lithography and the wet-etching process to create the semiconductor islands and the vias. Next, 80-nm-thick ITO was deposited by RF sputtering and structured by liftoff to form the source–drain contacts. Finally, the devices were passivated with an additional 25-nm-thick Al_2O_3 layer.

B. Device and Circuits Structure

All TFTs utilized a ground-signal-ground (GSG) contact pad layout, as shown in Fig. 1(b). This allows their reliable ac characterization through GSG probe tips. Circuits were designed based on nMOS circuit typologies consisting in n-type IGZO TFTs in a diode load configuration as active load element. The minimum feature size, and hence minimum channel length, that can be obtained with the described fabrication process was 4.5 μm. Interconnections and contact pads within circuits were realized through the gate, and source/drain ITO layers structuring of the TFTs fabrication process without the need for additional process steps or lithography masks and no additional metal layer was overlaid.

C. Transparency

As shown in Fig. 1(b), the fabricated devices were virtually invisible on the partially transparent polyimide substrate. Transmittance measurements of the full electronics stack and the substrate were performed in the visible (VIS) and near-infrared (NIR) range (450–900 nm) to verify their optical properties. Measurements at shorter wavelengths were not reliable because of the strong absorption of the substrate, which can be seen from its yellowish color. Fabrication and characterization of transparent TFTs on this substrate are still relevant, as the used polyimide foil is by far the most common substrate for the fabrication of flexible thin-film devices. Nevertheless, future studies can investigate the suitability of other substrates with the proposed fabrication process for the development of fully transparent and flexible devices [18], [19], [23]. The measurement was performed using an Agilent Cary 5000 UV–VIS–NIR spectrum analyzer. The device transmittance spectra shown in Fig. 1(c) were normalized by the transmittance of the polyimide substrate and confirm the practical full transparency of the transistors. The normalized values above 100% are associated with the noise of the experimental setup that causes a transmittance variation for the TFTs of ±1.56%.

III. Results and Discussion

All measurements were carried out in a probe station in ambient conditions.

A. Transistors

The dc characterization of TFTs, consisting in both voltage–current curves and capacitance–voltage curve, was performed by a Keysight B1500A parameter analyzer. The ac performance was evaluated by measuring the scattering parameters by a Keysight E5061B ENA network analyzer.

1) Electrical Characterization: The transfer characteristics of a representative transparent IGZO TFT is shown in Fig. 1(d). The measurement shows the TFT in the linear region $V_{DS} = 0.1$ V and in the saturation region $V_{DS} = 5$ V. The corresponding output characteristics are shown in Fig. 1(e). Following the Shichman–Hodges model [24], the extracted electrical parameters are as follows: threshold voltage $V_{TH} = -0.76$ V, field-effect mobility $\mu_{eff} = 19.39\,cm^2\,V^{-1}\,s^{-1}$, subthreshold swing $SS = 334.55$ mV/dec, ON–OFF current ratio $I_{ON}/I_{OFF} = 2.24 \times 10^6$, maximum transconductance $g_m = 0.362$ mS, and output resistance $r_0 = 5.06\,k\Omega$ defining an internal gain $g_m/g_0 = 1.84$. These parameters are comparable to the ones extracted from state-of-the-art non-transparent flexible IGZO TFTs [25]–[28]. However, the transfer characteristics also shows signs of drain inducted barrier lowering effects caused by the short channel length, leading to a reduction of the V_{TH} and an increase in I_{OFF} with increasing V_{DS}. Capacitance–voltage measurements were performed to assess the gate capacitance C_G of the devices. These result in a decrease of the C_G in a frequency range from $f = 1$ kHz to $f = 1$ MHz [see Fig. 1(f)]. At $f = 1$ MHz, the gate-to-drain overlap capacitance is 2.13 pF, and the total measured gate capacitance is 5.37 pF. This allows the theoretical calculation of the transit frequency f_t utilizing g_m and C_G that is calculated to be 10.7 MHz for the shown TFT. Scattering parameters of the TFTs were measured to evaluate the ac behavior of the devices and extract the values of f_t and the maximum oscillation frequency f_{max}. The dc bias points to perform the measurements were $V_{DS} = 5$ V and $V_{GS} = 3$ V. Fig. 2(a) and (b) shows the magnitude h_{21} and the imaginary part $1/h_{21}$ of the current gain for a TFT with $W/L = 50/4.5\,\mu$m (the same TFT as in Fig. 1). The graphs were obtained from the measured S-parameters shown in Fig. 2(c) and allowed to extract an $f_t \approx 7.84$ MHz. It is worth to

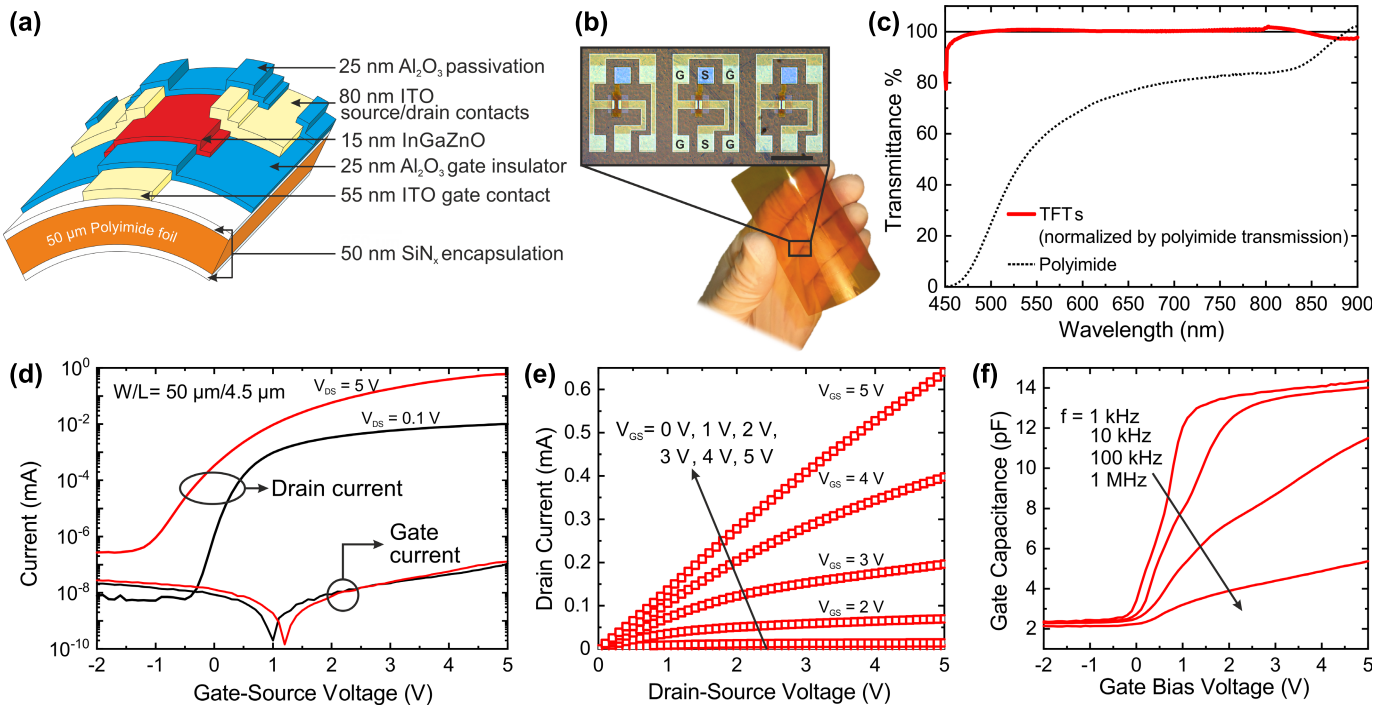

Fig. 1. Structure and performance of transparent IGZO TFTs. (a) Schematic, materials, and layer thicknesses of the flexible devices. (b) Micrograph of a TFTs array with a GSG design on a flexible polyimide substrate (scale bar: 250 μm). (c) Transparency measurements of TFTs in the VIS and NIR range. (d) Transfer and (e) output characteristics of a representative transparent TFT. (f) Gate capacitance dependence on frequency variation.

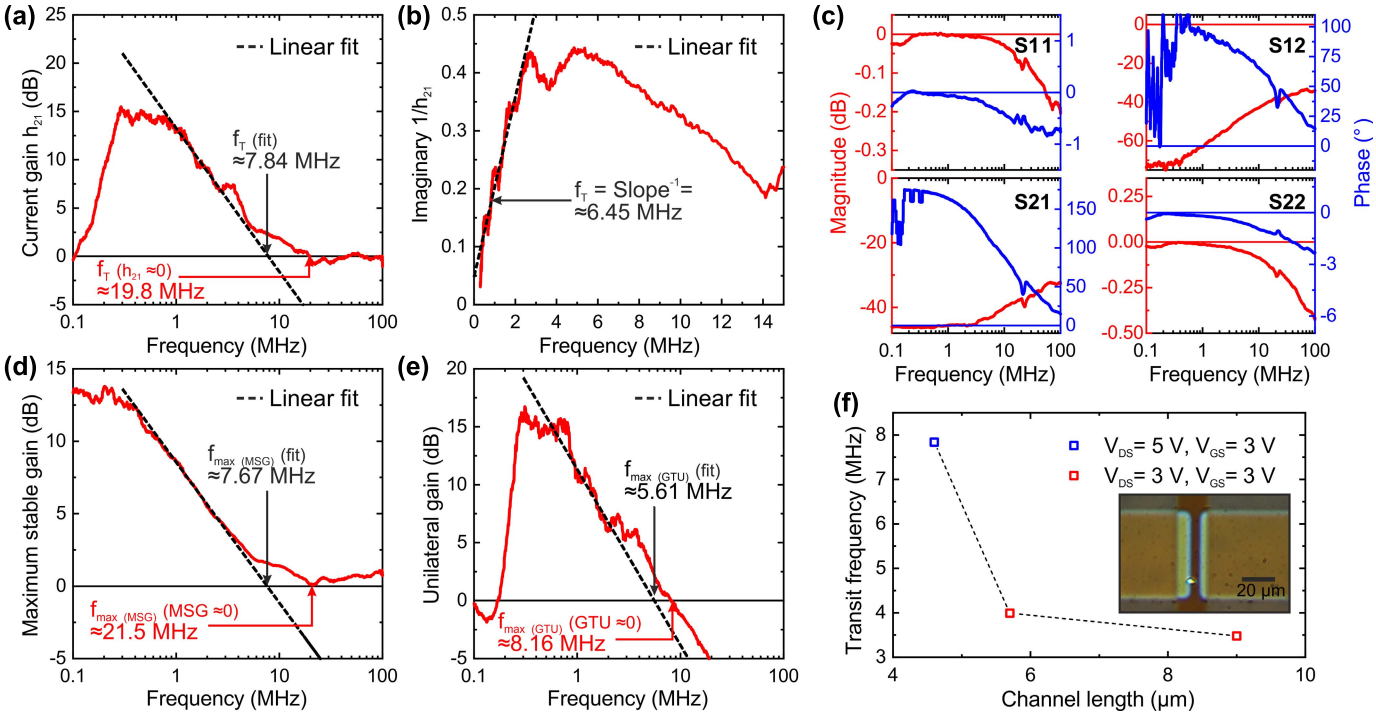

Fig. 2. AC performance of transparent IGZO TFTs on polyimide foil. (a) Current gain magnitude and (b) imaginary part of the current gain for a representative TFT showing the transit frequency f_t of the device. (c) Measured S-parameters for the TFT. (d) MSG and (e) GTU for the same TFT showing the maximum oscillating frequency f_{max} of the device. (f) Transit frequency variation as a function of the channel length. Inset: optical micrograph of the shortest TFT channel.

mention that f_t was extrapolated from the expected decreasing behavior of the current gain due to the frequency, whereas the actual measured unity gain frequency of the current gain is 19.8 MHz. This approach is validated by the alternative determination of f_t using the imaginary part of the current gain shown in Fig. 2(b) defining an $f_t \approx 6.45$ MHz [29].

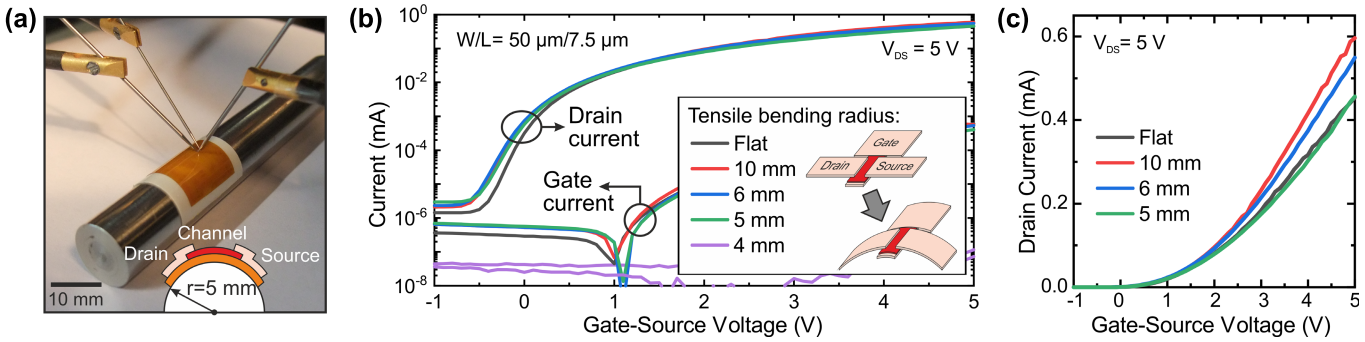

Fig. 3. Transparent IGZO TFTs functionality under bending condition. (a) Contacted flexible substrate bent to a radius of 5 mm. (b) Transfer characteristic of a TFT at V_{GS} = 5 V at different bending radii (4, 5, 6, and 10 mm) and comparison with flat device. Inset: tensile bending radius applied parallel to the TFT channel. (c) Transfer characteristics using a liner current scale showing the drain current dependence on bending in the on regime (V_{DS} = 5 V).

The value of $f_{\max}$ is also derived from the S-parameters according to the definition of the maximum stable gain (MSG) and the unilateral gain (GTU) [30] resulting in $f_{\max(MSG)} \approx 7.67$ MHz, whereas $f_{\max(GTU)} \approx 5.61$ MHz. The values are derived from a linear fit of the measured MSG and GTU, as shown in Fig. 2(d) and (e), respectively. Finally, the f_t dependence on the TFTs channel length is depicted in Fig. 2(f). In accordance with the theoretical formula of

$$f_t = \frac{g_m}{2\pi C_G} \tag{1}$$

the graph shows the reduction of f_t for longer device channels due to the scaling effects on both g_m and C_G [25].

2) Mechanical Performance: The electrical properties of an IGZO TFT ($W/L = 50/7.5\,\mu$m) were evaluated by characterizing the device while subjected to tensile mechanical strain parallel to the TFT channel [28]. Strain was created by bending the device to different radii between 10 and 4 mm. These radii correspond to strain values between 0.3% and 0.68%, calculated according to [31] and considering the built-in strain in the substrate. As displayed in Fig. 3(a), the substrate was attached to a rod with defined radius using a double sided tape and characterized while bent. The devices were re-flattened after each static bending. The transfer characteristics plotted in Fig. 3(b) represent the TFT performance under bending and in flat condition measured in the saturation regime (V_{DS} = 5 V). The V_{TH} value shifts toward the negative side, and μ_{eff} increases compared with the flat condition when bending the device down to 6 mm. At this radius, the threshold voltage variation ΔV_{TH} is equal to 0.046 V, and the mobility variation $\Delta\mu_{eff}$ is equal to 3 cm^2 V^{-1} s^{-1}. Although, at high bending radius (r = 10 mm), an increment of I_{DS} is denoted, as shown in Fig. 3(c), its degradation occurred due to an increase of the applied mechanical strain corresponding to a reduction of r down to 5 mm. At this low bending radii, the observed behavior is less predictable than the parameters shift measured in non-transparent IGZO TFTs [32]. This is explained by the use of brittle ITO as gate and source/drain contacts, which is sensitive to the formation of microcracks [14], [33]. Most importantly, the measurements confirm that the transparent TFTs stay fully functional even when bent to a radius as small as 5 mm and re-flattened. However, if bending radii below 4 mm are applied, the induced strain permanently destroys the device.

B. Circuits

Characterization of transparent IGZO circuits was performed at the probe station in ambient conditions. The supply voltage of both five-stage ROs and CSAs was provided by a parameter analyzer. The output signal of the circuits was analyzed by a Keysight DSOS054A oscilloscope with an input resistance of 1 MΩ and an input capacitance below 2 pF. In the case of the CSA, the input signal was generated by a Keysight 33500B wave generator and also observed by the oscilloscope.

1) Ring Oscillators: The schematic and the micrograph of the RO are shown in Fig. 4(a) and (b), respectively. This consists on a five-stage RO with a buffer stage and employs identical inverting stage consisting of a driving TFT with $W/L = 350/10\,\mu$m and a load TFT with $W/L = 35/10\,\mu$m. The performance was evaluated by sweeping the supply voltage V_{DD}, while monitoring the output signal. A minimum V_{DD} of 1.75 V was needed to observe an ac output signal that is, to the best of our knowledge, the lowest V_{DD} for transparent IGZO ROs [13], [20], [23]. Here, the peak-to-peak amplitude is equal to 0.038 V, and the observed oscillation frequency f_{osc} is 6.78 kHz. This corresponds to a propagation delay of 29.5 μs/stage. Next, V_{DD} was swept from 1.75 to 12.25 V using a step size of 0.25 V, and the corresponding f_{osc} values were recorded. The resulting V_{DD} dependence of the output frequency, the amplitude, and the output offset was shown in Fig. 4(c)–(e). Supply voltages above 12.25 V caused a gate dielectric breakdown and lost the functionality of the circuit. Representative output waveforms for V_{DD} = 1.75 V and V_{DD} = 10 V are shown in Fig. 4(f) and (g), respectively. Even at the lowest supply voltage, the output waveform is very symmetrical and nearly perfectly sinusoidal. As expected, the highest operation frequency was observed for the largest supply voltage of 12.25 V. Here, the circuit oscillates at 132.9 kHz and exhibits an output amplitude and a dc offset of 2.36 and 8.54 V, respectively. Consequently, the stage delay reaches values as low as 752 ns. This operating frequency is significantly higher than f_{osc} observed in another fully transparent IGZO five-stage RO fabricated on colorless polyimide [23].

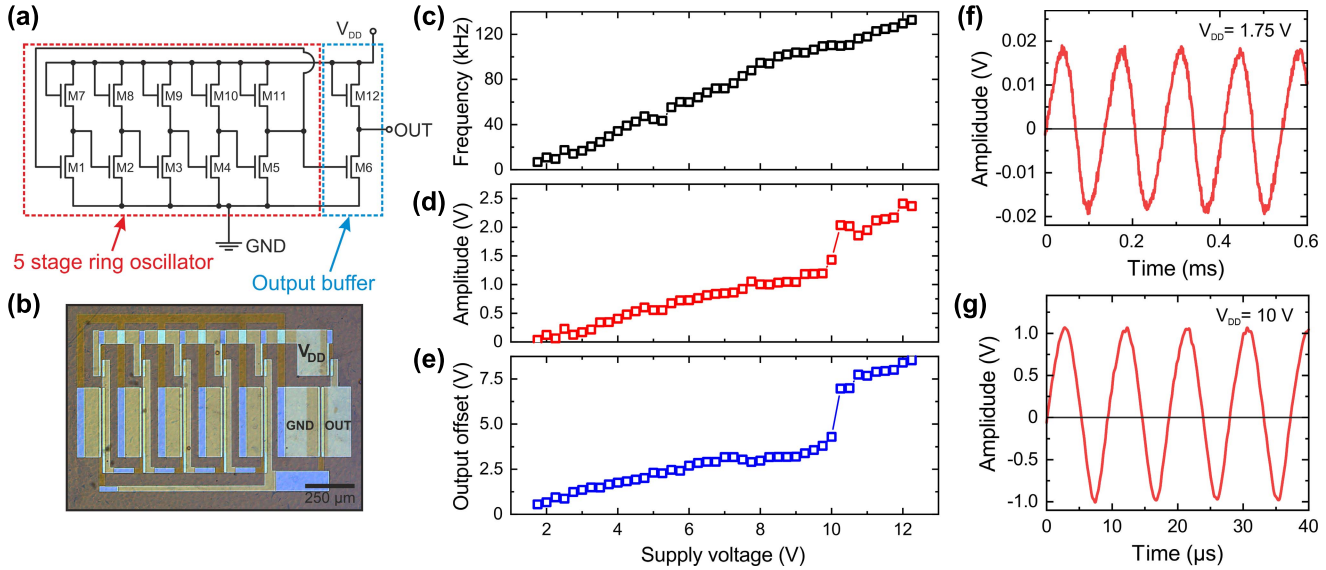

Fig. 4. Transparent five-stage RO. (a) Schematic and (b) optical micrograph of the five-stage RO with an output buffer stage. (c) Frequency, (d) amplitude, and (e) output offset dependence on supply voltage variation in the range between 1.75 and 12.5 V. Representative output waveforms for supply voltages of (f) 1.75 and (g) 10 V.

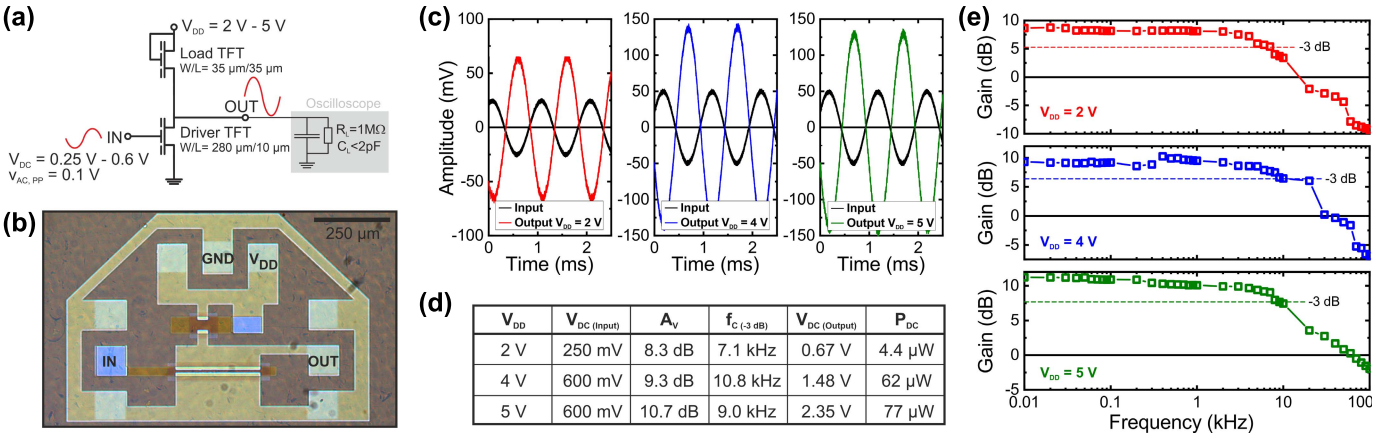

V_{DD}	$V_{DC\,(Input)}$	A_V	$f_{C\,(-3\,dB)}$	$V_{DC\,(Output)}$	P_{DC}
2 V	250 mV	8.3 dB	7.1 kHz	0.67 V	4.4 µW
4 V	600 mV	9.3 dB	10.8 kHz	1.48 V	62 µW
5 V	600 mV	10.7 dB	9.0 kHz	2.35 V	77 µW

Fig. 5. Transparent CSA. (a) Schematic and (b) optical micrograph of the transparent circuit. (c) Output and input amplitude for supply voltages V_{DD} of 2 V (red), 4 V (blue), and 5 V (green). (d) Table summarizing the electrical parameters of the circuit at the different V_{DD} values. (e) Bode plots of the circuit for different V_{DD} values: 2 V (red), 4 V (blue), and 5 V (green).

2) Common-Source Amplifier: The characterization of a fully integrated inverting common-source voltage amplifier is shown in Fig. 5. The schematic is given in Fig. 5(a), while the micrograph in Fig. 5(b) shows the fabricated circuit. Here, the driver TFT has a W/L ratio of 280/10 μm, and the load TFT has a W/L ratio of 25/25 μm. The CSA performance was analyzed at three supply voltages. The peak-to-peak amplitude of the input signal was $V_{ac} = 0.1$ V, and the dc offset was V_{dc} of 250 mV at $V_{DD} = 2$ V, 600 mV at $V_{DD} = 4$ V, and $V_{DD} = 5$ V. Fig. 5(c) illustrates the input and measured output waveforms at each V_{DD}, confirming the inverting behavior of the circuit and virtually no distortion of the signal. At the same time, the frequency response of the circuit is characterized by the Bode plots in Fig. 5(e). The cutoff frequency f_c (−3 dB frequency) and the unity gain frequency f_0 were extracted from those measurements. A $f_c = 7.1$ kHz and a low frequency voltage gain $A_v = 8.3$ dB were obtained at $V_{DD} = 2$ V. Also, the power consumption of the circuit reached a very low value of only 4.4 μW at this voltage. This proves the low voltage and power consumption operation of the circuit, and its suitability for front-end conditioning of wearable sensors. Subsequently, the increase in V_{DD} improved the operating frequency range of the CSA, since f_0 increases from 16.2 kHz at $V_{DD} = 2$ V to 63.2 kHz at $V_{DD} = 5$ V. The most important performance parameters are also summarized in Fig. 5(d). These measurements result in the gain bandwidth products of 18.5, 31.5, and 30.8 kHz for the three different supply voltages. At the same time, the gain and cutoff frequency only show marginal improvement if V_{DD} is increased, demonstrating that the operation of the circuit is mostly independent of the supply voltage. The obtained performance can be compared with the one of another flexible CSA fabricated using opaque materials, providing $f_c = 11.5$ kHz and $A_v = 8.0$ dB [34]. Other flexible opaque CSAs have also been reported showing similar A_v [35],

while improved f_c up to $f_c = 3.4\,\text{MHz}$ can be achieved by optimized circuit design [25], [36].

IV. Conclusion

We present the fabrication and comprehensive ac characterization of fully transparent and flexible TFTs, as well as integrated ROs and CSAs. TFTs are characterized by a transit frequency of 7.84 MHz, and their functionality at bending radii down to 5 mm is reported. For the ROs, a maximum oscillation frequency of 132.9 kHz and a functionality at a supply voltage as low as 1.75 V are shown. CSAs present a maximum voltage gain of 10.7 dB with a cutoff frequency of 9 kHz when measured at a supply voltage $V_{DD} = 5\,\text{V}$. Furthermore, the two circuits provide low voltage operation and low power consumption, making them suitable for sensors readout and on-site conditioning of wearable systems. The performance presented here, combined to the transparency of the devices, supports the devices implementation for backplanes of flexible displays as well as imperceptible epidermal patches.

References

[1] P. Heremans *et al.*, "Mechanical and electronic properties of thin-film transistors on plastic, and their integration in flexible electronic applications," *Adv. Mater.*, vol. 28, no. 22, pp. 4266–4282, Jun. 2016.

[2] F. Catania, H. De Souza Oliveira, P. Lugoda, G. Cantarella, and N. Münzenrieder, "Thin-film electronics on active substrates: Review of materials, technologies and applications," *J. Phys. D, Appl. Phys.*, vol. 55, no. 32, Apr. 2022.

[3] J. C. Costa, F. Spina, P. Lugoda, L. Garcia-Garcia, D. Roggen, and N. Münzenrieder, "Flexible sensors—From materials to applications," *Technologies*, vol. 7, no. 2, p. 35, Apr. 2019, doi: 10.3390/technologies7020035.

[4] J. Yoon *et al.*, "Robust and stretchable indium gallium zinc oxide-based electronic textiles formed by cilia-assisted transfer printing," *Nature Commun.*, vol. 7, no. 1, pp. 1–10, Jun. 2016.

[5] W.-H. Yeo *et al.*, "Multifunctional epidermal electronics printed directly onto the skin," *Adv. Mater.*, vol. 25, pp. 2773–2778, May 2013.

[6] P. Won *et al.*, "Stretchable and transparent kirigami conductor of nanowire percolation network for electronic skin applications," *Nano Lett.*, vol. 19, no. 9, pp. 6087–6096, Sep. 2019.

[7] C. I. Park *et al.*, "World's first large size 77-inch transparent flexible OLED display," *J. Soc. Inf. Disp.*, vol. 26, no. 5, pp. 287–295, May 2018.

[8] Y. Li, G. Xu, C. Cui, and Y. Li, "Flexible and semitransparent organic solar cells," *Adv. Energy Mater.*, vol. 8, no. 7, Mar. 2018, Art. no. 1701791.

[9] K. Nomura, H. Ohta, A. Takagi, T. Kamiya, M. Hirano, and H. Hosono, "Room-temperature fabrication of transparent flexible thin-film transistors using amorphous oxide semiconductors," *Nature*, vol. 432, no. 4016, pp. 488–492, Nov. 2004, doi: 10.1038/nature03090.

[10] H. Yabuta *et al.*, "High-mobility thin-film transistor with amorphous $InGaZnO_4$ channel fabricated by room temperature RF-magnetron sputtering," *Appl. Phys. Lett.*, vol. 89, no. 11, Sep. 2006, Art. no. 112123.

[11] L. Petti *et al.*, "Metal oxide semiconductor thin-film transistors for flexible electronics," *Appl. Phys. Rev.*, vol. 3, no. 2, Jun. 2016, Art. no. 021303, doi: 10.1063/1.4953034.

[12] K. Nomura, A. Takagi, T. Kamiya, H. Ohta, M. Hirano, and H. Hosono, "Amorphous oxide semiconductors for high-performance flexible thin-film transistors," *Jpn. J. Appl. Phys.*, vol. 45, no. 5B, pp. 4303–4308, 2006.

[13] A. Suresh, P. Wellenius, V. Baliga, H. Luo, L. M. Lunardi, and J. F. Muth, "Fast all-transparent integrated circuits based on indium gallium zinc oxide thin-film transistors," *IEEE Electron Device Lett.*, vol. 31, no. 4, pp. 317–319, Mar. 2010.

[14] G. A. Salvatore *et al.*, "Wafer-scale design of lightweight and transparent electronics that wraps around hairs," *Nature Commun.*, vol. 5, no. 2982, pp. 1–8, Jan. 2014.

[15] G. Cantarella *et al.*, "Buckled thin-film transistors and circuits on soft elastomers for stretchable electronics," *ACS Appl. Mater. Interfaces*, vol. 9, no. 34, pp. 28750–28757, Aug. 2017.

[16] H. J. Luo, P. Wellenius, L. Lunardi, and J. F. Muth, "Transparent IGZO-based logic gates," *IEEE Electron Device Lett.*, vol. 33, no. 5, pp. 673–675, Mar. 2012.

[17] Y. Rim, H. Chen, Y. Liu, S. Bae, H. Kim, and Y. Yang, "Direct light pattern integration of low-temperature solution-processed all-oxide flexible electronics," *ACS Nano*, vol. 8, no. 9, pp. 9680–9686, Sep. 2014.

[18] H. Ning *et al.*, "Transparent flexible IGZO thin film transistors fabricated at room temperature," *Membranes*, vol. 12, no. 1, p. 29, Dec. 2021.

[19] G. J. Lee, J. Kim, J.-H. Kim, S. M. Jeong, J. E. Jang, and J. Jeong, "High performance, transparent a-IGZO TFTs on a flexible thin glass substrate," *Semicond. Sci. Technol.*, vol. 29, no. 3, Jan. 2014, Art. no. 035003.

[20] M. Mativenga, M. H. Choi, J. W. Choi, and J. Jang, "Transparent flexible circuits based on amorphous-indium–gallium–zinc–oxide thin-film transistors," *IEEE Electron Device Lett.*, vol. 32, no. 2, pp. 170–172, Dec. 2010.

[21] L.-Y. Su and J. Huang, "Demonstration of radio-frequency response of amorphous IGZO thin film transistors on the glass substrate," *Solid-State Electron.*, vol. 104, pp. 122–125, Feb. 2015.

[22] N. Münzenrieder *et al.*, "Flexible self-aligned double-gate IGZO TFT," *IEEE Electron Device Lett.*, vol. 35, no. 1, pp. 69–71, Jan. 2014, doi: 10.1109/LED.2013.2286319.

[23] H.-H. Hsieh, C.-H. Wu, C.-C. Wu, Y.-H. Yeh, H.-L. Tyan, and C.-M. Leu, "P-11: Amorphous In_2O_3-Ga_2O_3-ZnO thin film transistors and integrated circuits on flexible and colorless polyimide substrates," in *SID Symp. Dig. Tech. Pap.*, vol. 39, no. 1, May 2008, pp. 1207–1210.

[24] H. Shichman and D. A. Hodges, "Modeling and simulation of insulated-gate field-effect transistor switching circuits," *IEEE J. Solid-State Circuits*, vol. SSC-3, no. 3, pp. 285–289, Sep. 1968, doi: 10.1109/JSSC.1968.1049902.

[25] N. Münzenrieder *et al.*, "Contact resistance and overlapping capacitance in flexible sub-micron long oxide thin-film transistors for above 100 MHz operation," *Appl. Phys. Lett.*, vol. 105, no. 26, Art. no. 263504, Dec. 2014, doi: 10.1063/1.4905015.

[26] S. Nakano *et al.*, "Highly reliable a-IGZO TFTs on a plastic substrate for flexible AMOLED displays," *J. Soc. Inf. Display*, vol. 20, no. 9, pp. 493–498, Sep. 2012.

[27] C.-W. Chien *et al.*, "High-performance flexible a-IGZO TFTs adopting stacked electrodes and transparent polyimide-based nanocomposite substrates," *IEEE Trans. Electron Devices*, vol. 58, no. 5, pp. 1440–1446, Feb. 2011.

[28] N. Munzenrieder, C. Zysset, T. Kinkeldei, and G. Troster, "Design rules for IGZO logic gates on plastic foil enabling operation at bending radii of 3.5 mm," *IEEE Trans. Electron Devices*, vol. 59, no. 8, pp. 2153–2159, Aug. 2012.

[29] H. K. Gummel, "On the definition of the cutoff frequency fT," *Proc. IEEE*, vol. 57, no. 12, p. 2159, Dec. 1969.

[30] N. Münzenrieder *et al.*, "Flexible InGaZnO TFTs with f_{max} above 300 MHz," *IEEE Electron Device Lett.*, vol. 39, no. 9, pp. 1310–1313, Jul. 2018, doi: 10.1109/LED.2018.2854362.

[31] H. Gleskova, S. Wagner, and Z. Suo, "A-Si: H thin film transistors after very high strain," *J. Non-Crystalline Solids*, vol. 266, pp. 1320–1324, Mar. 2000, doi: 10.1016/S0022-3093(99)00944-8.

[32] N. Munzenrieder, K. H. Cherenack, and G. Troster, "The effects of mechanical bending and illumination on the performance of flexible IGZO TFTs," *IEEE Trans. Electron Devices*, vol. 58, no. 7, pp. 2041–2048, Jul. 2011, doi: 10.1109/TED.2011.2143416.

[33] K. Park *et al.*, "Stretchable, transparent zinc oxide thin film transistors," *Adv. Funct. Mater.*, vol. 20, no. 20, pp. 3577–3582, Oct. 2010.

[34] N. Münzenrieder *et al.*, "Oxide thin-film electronics on carbon fiber reinforced polymer composite," *IEEE Electron Device Lett.*, vol. 38, no. 8, pp. 1043–1046, Jun. 2017.

[35] G. Cantarella *et al.*, "Review of recent trends in flexible metal oxide thin-film transistors for analog applications," *Flexible Printed Electron.*, vol. 5, no. 3, Aug. 2020, Art. no. 033001.

[36] N. Munzenrieder *et al.*, "Flexible a-IGZO TFT amplifier fabricated on a free standing polyimide foil operating at 1.2 MHz while bent to a radius of 5 mm," in *IEDM Tech. Dig.*, Dec. 2012, pp. 5.2.1–5.2.4.

Open Access funding provided by 'Libera Università di Bolzano' within the CRUI CARE Agreement